SCIENTIFIC REPORTS

OPEN

Location and Electronic Nature of Phosphorus in the Si Nanocrystal — SiO_2 System

Received: 24 September 2014
Accepted: 04 March 2015
Published: 22 May 2015

Dirk König[1,2], Sebastian Gutsch[3], Hubert Gnaser[4], Michael Wahl[4], Michael Kopnarski[5], Jörg Göttlicher[6], Ralph Steininger[6], Margit Zacharias[3] & Daniel Hiller[3]

Up to now, no consensus exists about the electronic nature of phosphorus (P) as donor for SiO_2-embedded silicon nanocrystals (SiNCs). Here, we report on hybrid density functional theory (h-DFT) calculations of P in the SiNC/SiO_2 system matching our experimental findings. Relevant P configurations within SiNCs, at SiNC surfaces, within the sub-oxide interface shell and in the SiO_2 matrix were evaluated. Atom probe tomography (APT) and its statistical evaluation provide detailed spatial P distributions. For the first time, we obtain ionisation states of P atoms in the SiNC/SiO_2 system at room temperature using X-ray absorption near edge structure (XANES) spectroscopy, eliminating structural artefacts due to sputtering as occurring in XPS. K energies of P in SiO_2 and SiNC/SiO_2 superlattices (SLs) were calibrated with non-degenerate P-doped Si wafers. *Ab−initio* **results confirm measured core level energies, connecting and explaining XANES spectra with h-DFT electronic structures. While P can diffuse into SiNCs and predominantly resides on interstitial sites, its ionization probability is extremely low, rendering P unsuitable for introducing electrons into SiNCs embedded in SiO_2. Increased sample conductivity and photoluminescence (PL) quenching previously assigned to ionized P donors originate from deep defect levels due to P.**

About 60 years ago, impurity doping of bulk Si was established to introduce majority charge carriers, creating p/n junctions as fundamental building blocks of Si-based electronic devices. The discovery of size-controlled solid-state growth of SiNCs from Si-rich SiO_2 (SiO_x)[1] led to discussions about conventional dopants in SiNC/SiO_2 systems. P is of particular interest due to high solubility and diffusivity in Si[2]. Detailed insight into the behaviour of P within the SiNC/SiO_2 material system is crucial. It clarifies whether conventional SiNC doping is able to further advance miniaturization of Si-based electronic structures and electronic SiNC manipulation.

Many works have claimed doping of SiNCs with P donors[3–8], but very few provided unambiguous evidence and detailed data on doping probabilities[9,10] as gauge for working (active) dopants. Experimental evidence of successful P doping in SiNC/SiO_2 samples like quantum dot solar cells[11] or standard capacitance-voltage curves requiring a bulk semiconductor space charge region[12] likely occur due to interconnected SiNC/amorphous Si networks[13] where conventional doping does work to some extent. SiNCs separated by ultrathin SiO_2 barriers are dominated by defect-assisted conduction[14], though electric conductivities can be tremendously increased by massive P incorporation in the 0.5 to 8 atom-% range (0.25 to $4 \times 10^{21}\,cm^{-3}$)[3–8]. Such high P concentrations enter the composition range of ternary compounds (SiO_xP_y) with different properties as compared to Si, SiO_x and SiO_2. We note that Pearson and Bardeen[15] observed the semiconductor to metal transition of bulk Si for donor (P) and acceptor (boron;

[1]Integrated Material Design Centre (IMDC), UNSW, Sydney, Australia. [2]School of Photovoltaic and Renewable Energy Engineering (SPREE), UNSW, Sydney, Australia. [3]Laboratory of Nanotechnology, Dept. of Microsystems Engineering (IMTEK), University of Freiburg, Germany. [4]Department of Physics and Research Center OPTIMAS, University of Kaiserslautern, Germany. [5]Institute for Surface and Thin Film Analysis (IFOS) Ltd., Kaiserslautern, Germany. [6]ANKA Synchrotron Radiation Facility, Karlsruhe Institute of Technology, Germany. Correspondence and requests for materials should be addressed to D.K. (email: dirk.koenig@unsw.edu.au)

B) concentrations around 0.25 atom-% ($1.25 \times 10^{20}\,cm^{-3}$). With P concentrations in the 0.5 to 8 atom-% range, clustering with dopant inactivation, defect formation and massive out-diffusion occur already in bulk type Si layers for structure sizes of $\leq$30 nm in ultra-large scale integration (ULSI)[16,17]. Local P density fluctuations in SiNCs prevent to provide exactly one active dopant per SiNC[18]. The vast majority of SiNCs are undoped and very few SiNCs have multiple dopants. Latter leads to significant random deterioration of their electronic properties by exchange coupling[19]. Massive P densities in SiNC systems lead to P localized in SiO_2, in SiO_x surrounding SiNCs and P gettered by dangling bonds (DBs) at NC interfaces, all being critical for the electronic structure. So far, unpaired electrons bound to P were investigated by electron paramagnetic resonance (EPR) at very low temperatures[9,10]. Thermal broadening of EPR resonances prevented measurements at room temperature ($T = 300$ K). XANES is not restricted to low temperatures and yields information on the electronic state of *all* P at $T = 300$ K. Excited P K shell electrons in XANES have tremendously increased mean free paths as compared to X-ray photoelectron spectroscopy (XPS) due to their high kinetic energy E_{kin}[20]. We boosted sampling depths further by using XANES in fluorescence yield mode, allowing for non-destructive probing depths three orders of magnitude above XPS values. Due to the low E_{kin} of P L-III shell electrons, XPS is extremely surface sensitive. Probing samples below their original surface by XPS requires sputtering off top material, introducing artefacts as function of chemical species like sputter yield and atom re-coordination and re-ordering.

We report on h-DFT calculations of P at central lattice and interstitial sites in completely OH-terminated SiNCs, of saturated P at the surface of such NCs, in $SiO_{0.9}$ as sub-oxide shell around SiNCs and in SiO_2, delivering insights into the specific electronic structure due to P. The spatial distribution of P atoms in $SiNC/SiO_2$ systems is derived from APT data and their statistical processing to yield the P distribution profile from the SiO_2 matrix to the interior of the SiNCs. We discuss P data from h-DFT and XANES together with P spatial statistics from APT and obtain a detailed picture of the electronic behaviour of prospective P donors depending on their positions and bond geometries in $SiNC/SiO_2$ systems. The 1s core level energies from h-DFT are used to assign XANES signals to respective P configurations in h-DFT approximants.

Results

Hybrid DFT calculations. Figure 1 shows optimized approximants of a SiO_2 reference (α-quartz), of SiO_2 with P on a central Si site (SiO_2:P), of a $SiO_{0.9}$ reference and of P-doped $SiO_{0.9}$ ($SiO_{0.9}$:P). Fig. 1 further shows optimized approximants of a fully OH-terminated SiNC of 15 Å size as NC reference (OH-SiNC), and this NC with saturated (penta-valent) P substituting a corner Si atom (OH-SiNC > $P(OH)_3$), an OH group on such corner Si atom (OH-SiNC-$P(OH)_4$) and a H atom at the OH group substituted by $P(OH)_4$ (OH-SiNC-O-$P(OH)_4$). Fig. 1 also shows optimized approximants of fully OH-terminated 15 Å SiNCs with P on a central Si lattice site (OH-SiNC-P[Si]) and on a central interstitial cite (OH-SiNC-P[is]). Interstitial P coordinates relative to its 1-nn Si atoms were used from experiment[21]. Convergence of structural optimization of the approximant was accepted for residual forces on interstitial P and its 1-nn Si atom (and all other atoms) of 309 μeV/Å (11.3 μHa/Å) which is ca. 1.3% of the convergence threshold of maximum residual forces, see to Methods section at end of article. The atomic displacement associated with this minute residual force was 0.0032 Å (0.32 pm) which is ca. 94% of the convergence threshold of residual displacements of 0.003403 pm – a rather large value for such residual force. This variance is an indication of a somewhat flat energy landscape. Thereby, it is rather difficult to calculate an exact diffusion path of interstitial P. This may explain why dopant atoms on Si lattice sites were considered in *ab-initio* thermodynamic diffusion simulations[22–25], but dopant atoms on interstitial positions were not included. Further details on DFT calculations can be found in the Methods section at the end of the article.

Electronic Structure of P in SiO_2. The SiO_2 HOMO-LUMO gap is 7.83 eV which is 89% of the experimental value of ca. 8.8 eV[26]. We consider P on tetragonal Si sites in SiO_2 and SiO. P is surrounded by SiO_2 at least to its 5th next neighbour (5-nn) atom. Oxidation enthalpies[27] are 916 kJ/mol (9.49 eV/Si atom) for the chemical reaction $Si + O_2 \rightarrow SiO_2$ and 1493 kJ/mol (7.74 eV/P atom) for the reaction $2P + 2^1/_2\,O_2 \rightarrow P_2O_5$, indicating that pentavalent P configurations ($P(-O-)_5$) should not be favoured over tetravalent Si ($Si(-O-)_4$), leaving P with a DB in analogy to P donors in bulk Si. The DB of P is strongly associated with α-HOMO and β-LUMO, describing one state with its two spin configurations α and β (Fig. 2a). We compare the energies of frontier MOs with HOMO and LUMO energies of the OH-SiNC reference (Fig. 2, green lines). The β-LUMO energy of SiO_2:P is 0.01 eV above the LUMO of the OH-SiNC approximant while the α-HOMO of SiO_2:P is 0.41 eV below the HOMO of the OH-SiNC approximant. The barrier height for electron (hole) transport is given by the conduction (valence) band offset between Si and SiO_2 of 3.2 eV (4.5 eV)[26]. These values show that P in SiO_2 reduces the transport barrier for electrons (holes) by 97% (85%), causing an extreme increase in electron conductivity and a considerably increased hole conductivity. These defect levels are an important electronic aspect of P in SiO_2: It causes a massive increase in SiO_2 conductivity while *not working* as a donor. Several works build their evidence of SiNC doping on conductivities increasing with P concentrations of 0.5 to 8 atom-%[3,4,6–8]. From the SiO_2:P approximant we get an atomic ratio of $P/\left(\sum\left[Si + O + {}^1/_4 H\right]\right) = 0.88$ atom-% P, whereby we consider H terminating outermost O bonds as 1/4 Si.

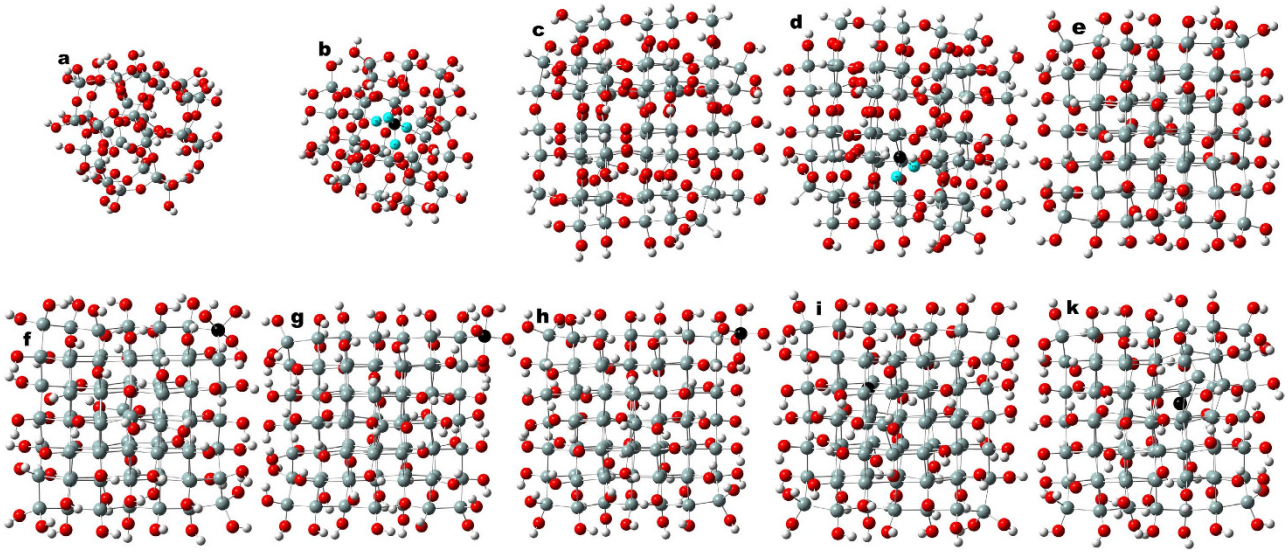

Figure 1. Optimized approximants calculated by h-DFT. Top row shows SiO_2 reference – $Si_{29}O_{40}(OH)_{36}$ (**a**), SiO_2:P – $Si_{28}PO_{40}(OH)_{36}$ (**b**), $SiO_{0.9}$ reference – $Si_{74}O_{55}(OH)_{35}H_{29}$ (**c**), $SiO_{0.9}$:P – $Si_{73}PO_{55}(OH)_{35}H_{29}$ (**d**) and fully OH-terminated 15 Å NC reference OH-SiNC – $Si_{84}(OH)_{64}$ (**e**). The bottom row shows OH-SiNC with corner $>Si(OH)_2$ substituted by $>P(OH)_3$ referred to as OH-SiNC$>P(OH)_3$ – $Si_{83}P(OH)_3(OH)_{62}$ (**f**), with OH group at corner Si atom substituted by $P(OH)_4$ referred to as OH-SiNC-$P(OH)_4$ – $Si_{84}P(OH)_4(OH)_{63}$ (**g**), with OH group at corner Si atom substituted by $OP(OH)_4$ referred to as OH-SiNC-O-$P(OH)_4$ – $Si_{84}OP(OH)_4(OH)_{63}$ (**h**), OH-SiNC with central Si atom substituted for tetravalent P referred to as OH-SiNC-P[Si] – $Si_{83}P(OH)_{64}$ (**i**), and with P on an interstitial site in the NC center referred to as OH-SiNC-P[is] – $Si_{84}(OH)_{64}$-is-P (**k**). Atom colors: Si is gray, P is black, O is red and H is white. 1-nn O atoms of P in SiO_2 and $SiO_{0.9}$ approximants shown in cyan. Approximants shown along [001] lattice vector group except SiO_2 and SiO_2:P.

Electronic Structure of P in SiO. Approximants for $SiO_{0.9}$ and $SiO_{0.9}$:P are based on α-quartz. Every second O bridge Si–O–Si is substituted by a bond Si–Si. As with SiO_2:P, we have a DB on P occupied with one electron in the $SiO_{0.9}$:P approximant at a central Si lattice site, again resulting in two different spin orientations per MO (α, β). Frontier MOs are similar to SiO_2:P, describing the DB of P with one electron occupying the α-HOMO. The α-HOMO – β-LUMO gap of 1.96 eV is 0.76 eV below E_{gap}=2.72 eV of the OH-SiNC reference. The HOMO in $SiO_{0.9}$:P is located 1.05 eV above the HOMO of the OH-SiNC reference. Hence, P presents a deep recombination center in SiO_x shells (Fig. 2b) which cover SiNCs with a thickness of 1 to 1.5 mono layers (MLs)[28]. This finding is supported by PL quenching reported for high P concentrations mentioned above[3,29].

The LUMO of $SiO_{0.9}$:P facilitates electron transport by diminishing the electron barrier. As for the SiO_2:P approximant, electron (hole) barriers are decreased down to 32% (removed completely). For $SiO_{0.9}$ and $SiO_{0.9}$:P approximants, a helical arrangement of Si atoms along the ⟨001⟩ vector (Fig. 1c,d) dominates MOs from $E - E_{vac} = 0.2$ to -8.5 eV. The inner bonds of these Si backbones can resist electron transfer to O to some extent, diminishing the splitting of their bonding and anti-bonding MOs. Experiments yield $E_{gap}(SiO) \approx 2.48$ eV[30], our calculations overestimate this value by 54%. This may be due to the very balanced local stoichiometry of the $SiO_{0.9}$ reference and $SiO_{0.9}$:P approximants as well as their high space group symmetry which allows for mentioned Si helices. Local Si segregation suggests that SiO is not uniform[13] which can lower the band gap. The P concentration can be calculated as for the SiO_2:P approximant, yielding 0.56 atom-% for $SiO_{0.9}$:P.

Electronic Structure: Saturated P at SiNC interfaces. Tetravalent P atoms substantially gain binding energy when gettering their DBs at NC interfaces and maximize binding energies of Si atoms providing DBs. It is thus energetically unfavourable for P at the NC interface to have a DB. This finding is supported by a maximum P density at SiNC interfaces derived from APT below.

We show the DOS of the OH-SiNC reference approximant along with the DOS of all three approximants containing bond-saturated P at the interface (Fig. 3). Fully gettered P at NC interfaces does not introduce defect levels within the HOMO-LUMO gap of the SiNC. The DOS of OH groups has an energy gap of 8.0 eV, corresponding to 91% of the experimental band gap of SiO_2[26]. The DOS of the SiNC approximants expose a small shift of HOMO and LUMO to higher binding energies, correlating with an increasing number of O atoms[31,39].

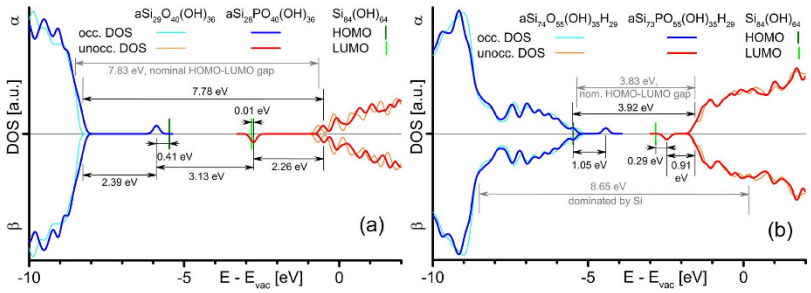

Figure 2. Electronic DOS of oxides containing P. Results for SiO_2:P (**a**) and $SiO_{0.9}$:P (**b**), shown with DOS of pure SiO_2 (top) and pure $SiO_{0.9}$ (bottom) approximants. Dark (bright) green lines show HOMO (LUMO) of OH-SiNC.

Electronic Structure of P within SiNCs. We consider P on a central Si lattice site OH-SiNC-P[Si] and on a central interstitial site OH-SiNC-P[is]. P on a Si lattice site generates a HOMO 0.51 eV below the LUMO energy (Fig. 4a). While this HOMO presumably becomes a donor state for vanishing quantum confinement, its ionization energy E_{ion}=0.51 eV is too big to ionize SiNCs with a reasonable probability at $T = 300$ K; $\mathcal{P}_{dope} = \exp(-E_{ion}/k_B T) = 2.7 \times 10^{-9}$. Even for SiNCs at the upper size limit of quantum confinement, $\mathcal{P}_{dope}$ will be too small for providing electrons to SiNCs; experimental values[10] for $d_{NC} \approx 90$ Å are $\mathcal{P}_{dope} \approx 4 \times 10^{-5}$. Interstitial P introduces two gap states, a HOMO 0.57 eV above the HOMO of the 1.5 nm SiNC and a LUMO 0.46 eV below the LUMO of the SiNC (Fig. 4b). Both states due to P cannot donate electrons but provide efficient carrier recombination with a transition energy of 1.72 eV. As this transition is optically active at a wavelength of ca. 720 nm, it must be considered for PL spectra of P-doped SiNC/SiO_2 species. Both cases of P in OH-SiNC introduce recombination levels into SiNCs.

Atom Probe Tomography. We show the APT scan of a SiNC SL in SiO_2 where SiNCs are enclosed by iso-surfaces with atomic concentrations of Si $N_{Si} \geq 0.7$, i.e. ≥70 atom-% Si (Fig. 5a). With the molar ratio of $Si/O = 1/2$ in SiO_2, we derive the molar SiO_2 partition P_{SiO_2} of SiNCs via $P_{SiO_2} = 1/2\, N_O/N_{Si}$ Ignoring the P partition of ca. 1 atom-%, we get $P_{SiO_2} \leq 21$ mol-% SiO_2 and $P_{Si} = 1 - P_{SiO_2} \geq 79$ mol-% Si for volumes enclosed by iso-surfaces. We note that the real P_{SiO_2} value is lower due to APT projection artefacts. Detailed statistical analyses of APT data[32] revealed that about 15% of the P atoms are found within SiNCs, whereas about 30% are trapped at the interface and about 55% reside in the surrounding SiO_2 matrix. This relatively low P concentration in SiNCs can be explained by self-purification[22–25], by solubilities of P in Si and SiO_2 and by the high relative SiO_2 volume of 85% in our samples. Zooming into the APT scan shows P atoms within SiNCs (Fig. 5b). A notable P concentration within SiNCs appears to disprove self-purification. However, interstitial P[21] should have a much higher probability to exist in SiNCs as compared to P built into SiNC lattice sites. It does not require bond breakage and can exploit the fast diffusivity and high saturation density of P. An inclusion of such P configurations into *ab-initio* thermodynamic diffusion simulations would complement existing self-purification models which only consider foreign atoms at SiNC lattice sites. Tomogram data from APT used for a cluster analysis[32] comprised numerous SiNCs in SiO_2:P. The resulting proxigram shows the radial concentration of Si, O and P (Fig. 5c). We found a strong accumulation of P atoms in the SiNC/SiO_2 interface shell with $SiO_{x\approx1}$ and also an increased P concentration within SiNCs.

XANES spectroscopy. We measure P K spectra to determine the P oxidation stage by its K shell electron binding energy (Fig. 6), using a non-degenerate P-doped Si wafer (donor density = 0.2 to 1×10^{19} cm^{-3} or 0.004 to 0.02 atom-%) for calibration. We assign XANES results to P environments using 1s core levels calculated by h-DFT with all-electron MO-BSs. P 1s core level energies from h-DFT correspond to 97.864% of P K XANES energies, see table 1. We calibrated h-DFT values by a factor of 1.02183 as supported by h-DFT P 1s core level energies of P_2O_5 (P^{+5}) and P_2O_3 (P^{+3}) approximants calculated with the same h-DFT route (Fig. 7).

Discussion

Origin of PL quenching of SiNCs containing P. Diffusion of P through Si proceeds at high rates during SiNC segregation anneal with $T \approx 1100$ °C. Experimental data shown above and DFT calculations[22–25] indicate that P appears to be within SiNCs on interstitial sites with a probability of nearly 100%. Auger recombination was assumed to cause PL quenching in SiNC/SiO_2 material systems with high P concentrations[3]. Our findings do not support this assumption. With extremely low P ionization probabilities, the difference in free carrier densities of doped and intrinsic SiNCs is virtually nil. The Auger

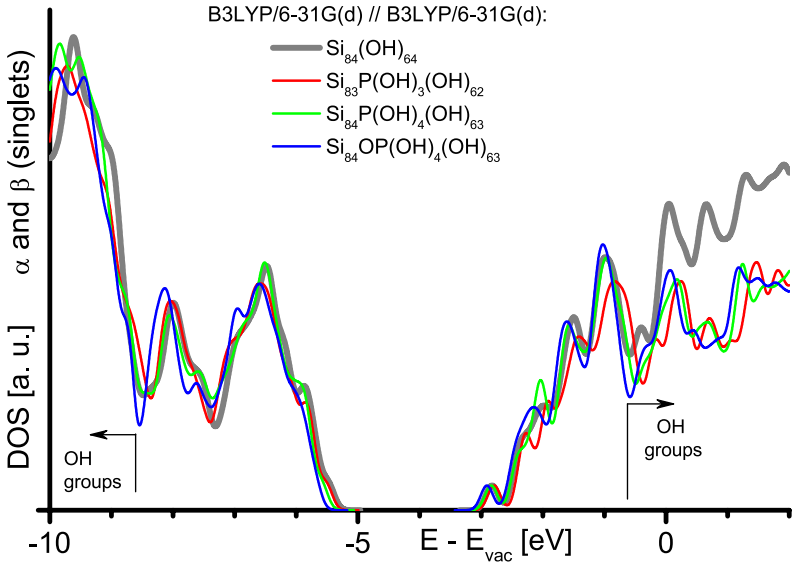

Figure 3. Electronic DOS of SiNCs with P at interface. Data of OH-SiNC reference ($Si_{84}(OH)_{64}$) and its versions with bond-saturated P at NC interface, see Figure 1 for details.

recombination $\mathcal{R}_{Aug}$ rate is[33,34] $\mathcal{R}_{Aug} = N_{Aug}(n^2p + p^2n)$, where n (p) are the density of free electrons (holes) and N_{Aug} is the Auger scattering coefficient ($\approx 10^{-31}$ cm^6/s for bulk Si[34]). Under high injection conditions ($n = p$), Auger recombination is $\propto n^3$ which explains its strong increase at high free carrier densities[35,36]. P located within SiNCs or within SiO_x shells around SiNCs are deep defect centers which appear to provide the most efficient and fastest path for non-radiative carrier recombination. This process explains PL quenching already at reasonably high P densities[29] still below values reported elsewhere[3,4]. Co-doping with B was shown in experiment to *increase* PL intensities while transition energies decreased below those of undoped SiNCs[3]. Localized states of B and P at or within SiNCs provide strong radiative transitions as donor electrons directly relax into acceptor states. PL energies decreasing with co-doping [37] are a clear indication of this mechanism.

P ionization in SiNC/SiO_2 samples. P in bulk Si has four bonds to its 1-nn Si atoms, acquiring 0.09 electrons (2.2% bond ionicity). The P charge is −0.09 for neutral donors and +0.91 for ionized donors. P donors in bulk Si have E_{ion}=0.049 eV[38], yielding a doping (ionization) probability at T = 300K of $\mathcal{P}_{dope} = \exp(-E_{ion}/k_BT) = 0.15$. The average charge of all P atoms in bulk Si is then $-0.09 \times (1 - 0.15) + 0.91 \times 0.15 = +0.06$, corresponding to oxidation stage zero (P^0). This value refers to the XANES peak at 2144.8 eV of the P doped Si wafer reference (Si:P), see Fig. 6. All P-doped SiNC/SiO_2 samples (2 to 5 nm SiNC/SiO_2 SLs, bulk) show peaks at 2143.7 eV. The 1.1 eV shift to lower binding energies shows that P in SiNC/SiO_2 is much less positively ionized, corresponding to P^{-1}. This result is corroborated by the Mulliken charges of P obtained from h-DFT and the analytical value of P in bulk Si (table 1). A hint of a signal shoulder might exist for all SiNC samples at the XANES peak for P^0 at 2144.8 eV. An indication of a signal occurs for the smallest SiNC size of 2 nm, suggesting a slightly increased doping probability for ultrasmall SiNCs also observed by EPR[10], though the ultrasmall SiNC size notably increases the signal background for XANES and presumably EPR. Our results show that P does not provide electrons to SiNCs embedded in SiO_2 with reasonable probabilities.

Conclusion

We carried out DFT calculations for the SiNC/SiO_2 system to monitor the electronic nature of P. On a lattice site within OH-terminated SiNCs, P introduces a deep donor level with E_{ion} = 0.51 eV; ionisation for small SiNCs is virtually nil, but is likely to increase for SiNCs with diminishing quantum confinement. However, formation energies of P on Si lattice sites[22–24] suggest that P in SiNCs occurs almost exclusively on interstitial sites which is indirectly corroborated by experiments showing an extremely small density of P atoms with unpaired electrons even for 10 nm SiNCs[9,10]. On a central interstitial site within SiNCs, P cannot donate an electron (E_{ion} > 2 eV), but forms two deep defect levels with a recombination transition at 1.72 eV. At SiNC interfaces, fully saturated P have no impact on frontier molecular orbitals, leaving HOMO and LUMO energies virtually unchanged. In SiO shells around SiNCs, P is again unable to donate an electron, but induces a deep defect level which triggers massive recombination. This defect causes PL quenching – as opposed to Auger recombination – and increases SiO shell conductivities which were both interpreted as evidence for successful SiNC doping in the literature[3,8]. Although

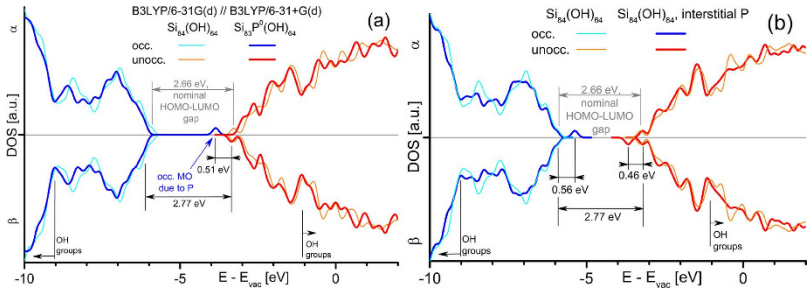

Figure 4. Electronic DOS of OH-SiNC approximant with P residing inside SiNC. P located on a central Si substitutional site (**a**) and on a central interstitial site (**b**), shown with DOS of reference OH-SiNC approximant.

P atoms in SiO_2 are deep defects which cannot donate electrons, they tremendously improve inter-NC conductivities in particular for electrons by diminishing electron (hole) barriers by 97% (85%) of the conduction (valence) band offset between bulk phases of Si and SiO_2. Massively increased conductivities were assumed to prove successful SiNC doping[6,8]. APT analyses revealed an enrichment of P at SiNC interfaces, which appears to be due to DB saturation and support h-DFT analyses of fully O-saturated P at SiNC interfaces. SiNCs were found to contain significant amounts of P. While this appears to contradict self-purification theory, interstitial P with considerably more favourable thermodynamics and its high diffusivity and saturation density has not been considered in self-purification modeling. Core level (K shell) electron energies of P in SiO_2 and $SiNC/SiO_2$ samples were measured by XANES at room temperature. In contrast to bulk Si, P atoms in $SiNC/SiO_2$ samples could not donate electrons into 2 to 5 nm size NCs in SLs or in annealed bulk SiO_x films with reasonable probabilities, confirming our h-DFT results. We conclude that conventional doping of SiNCs with P does not provide majority charge carriers to SiNCs embedded in SiO_2. Alternative approaches for majority carrier introduction into embedded SiNCs and ultrasmall Si nanovolumes such as embedding material effects[39] have to be explored to advance SiNC-based nanoelectroncis and ULSI.

Methods

Sample Preparation. Size-controlled SiNCs in SiO_2 were fabricated by deposition of P-doped Si-rich oxide ($SiO_{0.93}$)/ intrinsic SiO_2 SLs by plasma enhanced chemical vapor deposition and subsequent annealing (1150 °C, 1 h). During deposition, P was incorporated by adding 1% PH_3 to Ar, resulting P concentrations were ca. 1 atom-% as found by secondary ion mass spectroscopy (SIMS)[29,32]. All samples were fabricated on low B-doped Si wafers (20 Ωcm) with 30 nm SiO_2 layers to prevent P diffusion into Si substrates during anneal. For APT, P doped SLs with 30 bilayers and 5 nm nominal NC size were fabricated. Samples with 50 bilayers and nominal NC sizes from 2 to 5 nm in steps of 1 nm were chosen for XANES. In addition, 300 nm thick P-doped SiO_2 and $SiO_{0.93}$ samples were fabricated as references.

Hybrid Density Functional Theory (h-DFT) Calculations. Approximants were calculated with non-periodic boundary conditions and underwent geometrical optimization with the B3LYP h-DF[40,41] and the 6-31G(d) all-electron molecular-orbital basis set (MO-BS)[42–44] using the GAUSSIAN 03 and GAUSSIAN 09 suites[45,46]. RMS and peak force convergence limits were 15.4 meV/Å (5.67×10^{-4} Ha/Å) and 23.1 meV/Å (8.51×10^{-4} Ha/Å), respectively. Electronic structures were computed with the same route; B3LYP/6-31G(d) // B3LYP/6-31G(d). Additional information is available on accuracy tests and tests of functional group termination as approximation of the dielectric[31,39,47]. During all calculations, no MO symmetry constraints were applied and tight convergence criteria were set for the self-consistent field routine.

Alternative approaches to the B3LYP h-DF with similar accuracy are the Heyd-Scuseria-Ernzerhof h-DF (HSE06)[48] and the Becke-Johnson exchange potential[49,50], latter used within the Perdew-Burke-Ernzerhof (PBE) DF[51] generalized gradient approximation (GGA) scheme.

Characterisation. We examined the position of P within the $SiNC/SiO_2$ system by APT using a Cameca LEAP 4000X HR instrument with a reflectron-type time-of-flight mass spectrometer and a pulsed UV laser (355 nm, 10 ps pulse length, 70 pJ pulse energy, 100 kHz repetition rate). During the analyses (chamber pressure 1×10^{-11} mbar), specimens were cooled to temperatures of around 76 K. The mass resolution of the system was $m/\Delta m \approx 800$, around 36% of all atoms are detected. Specimen tips have been prepared by the cut-and-lift-out technique using an ALTURA 875 dual-beam Focused Ion Beam instrument[32].

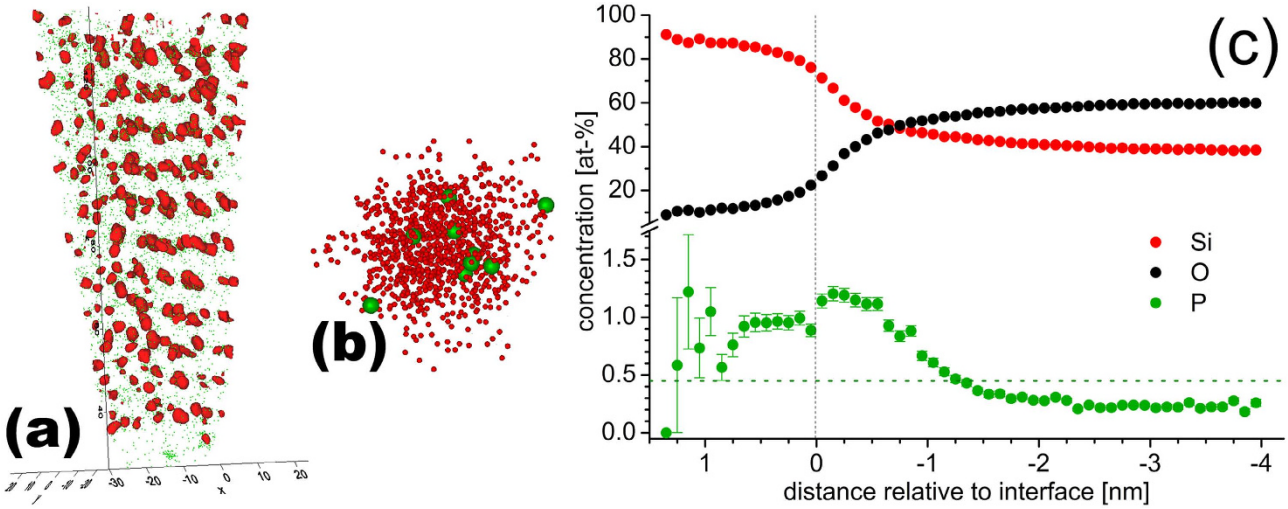

Figure 5. P-doped SiNC SL in SiO_2 scanned by APT. Composition of SL, volumes with ≥70 atom-% Si are covered by red iso-surfaces, individual P atoms are shown in green (**a**). P atoms within 3 nm SiNC (**b**). Proxigram derived from SiNCs in left graph, showing radial concentration distribution of Si, O and P, latter with error bars for standard deviation (**c**). Zero of distance scale defined by interface located at $SiO_{0.3}$ (85 mol-% Si and 15 mol-% SiO_2, ignoring P content). Concentrations scanned along normal vector of interface into SiNCs, stopping at center of smallest SiNCs (size ca. 2.7 nm) to avoid signal back-folding. Horizontal dashed line shows average P concentration.

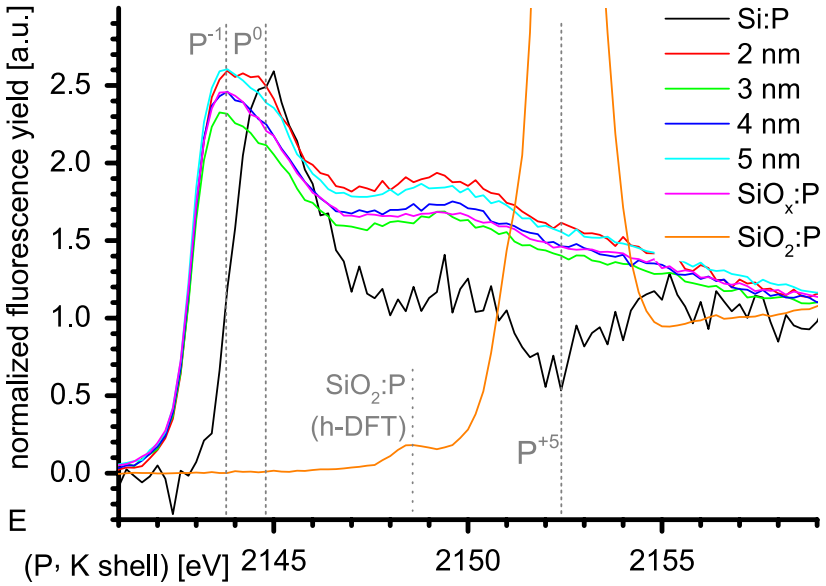

Figure 6. XANES spectra of SiNC/SiO_2 samples. Normalized K shell spectra of P in SiNC/SiO_2 SLs (2 nm, 3 nm, 4 nm, 5 nm), annealed bulk SiO_x sample SiO_x:P and P doped SiO_2 sample SiO_2:P shown together with doped Si wafer Si:P. Dashed gray lines show P oxidation stages.

The P K-edge absorption in XANES was measured at the SUL-X beamline at the Angströmquelle Karlsruhe (ANKA). Monochromatic X-rays were obtained using a Si(111) double crystal monochromator with an energy resolution of about 0.2 eV at 2150 eV with fixed exit. Scans were carried out using a shallow incident angle to maximize the SL or thin layer volume of samples for excitation. Absorption was measured by monitoring the P Kα fluorescence emission using a seven element Si(Li) fluorescence detector (SGX Sensortech). The signal is normalized to the incident photon flux measured simultaneously by a custom made ionization chamber (ADC, US) filled with N_2 at a pressure of 50 mbar. Energies

E (eV) (XAS, DFT)	$q(e^a)$	samples/ approximant	1-nn O of P; valence state[b]	remarks
2152.4		SiO_2:P (major)	5; V	also assigned to O=P(–O–)$_3$[53]
2150.8	+1.98	P_4O_{10} cage (2 P_2O_5)	4; V	
2149.4	+1.42	OH-SiNC-O-P(OH)$_4$	5; V	charge transfer to –**O**–P(OH)$_4$
2148.6↓	+1.29	SiO_2:P	4; IV	P in center with DB
2148.6		SiO_2:P (minor)	4; IV	
2148.3	+1.17	OH-SiNC-P(OH)$_4$	4; V	P directly on NC, four OH on P
2147.5	+1.02	P_4O_6 cage (2 P_2O_3)	3; III	fully occupied 3s↓↑ AO on P
2146.8	+0.94	OH-SiNC>P(OH)$_3$	3; V	P Si NC corner, >Si(OH)2→>P(OH)$_3$
2146.0	+0.51	$SiO_{0.9}$:P	2; IV	P in center with DB
2144.8	+0.06	P in bulk Si	0; IV	DB on P, 15% donors ($P^{+0.06}$)
2144.5↓	−0.28	OH-SiNC-P[Si]	0; IV	P with DB on Si site in NC center
2143.7		P in SiNCs	0; ??	all SiNC sizes, SL and bulk SiO_x samples
2142.9↑	−0.35	OH-SiNC-P[is]	0; 0	interstitial P(3s↑↓, 3p↑$_0$↑$_{+1}$↑$_{-1}$), NC center

Table 1. Core level energies of P (1s from h-DFT, K shell from XANES). Bold numbers present XANES values, underlined numbers indicate approximants with same or similar configuration to samples indicated by arrow. Further shown are P atomic charges, P configuration (DFT approximant, XANES sample), number of P 1−nn O atoms, P valence state and remarks. [a]Values are Mulliken charges for DFT approximants and derived analytically for P in Si wafer (see text). [b]P valence state is zero (0), tri (III), tetra (IV), penta (V) or unknown (??)

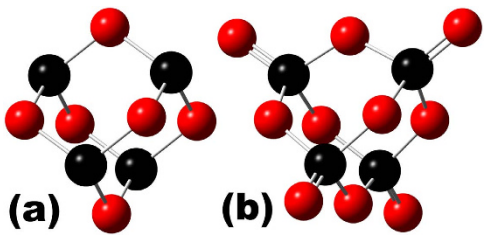

Figure 7. P_2O_3 and P_2O_5 approximants for XANES calibration. Approximants of P_4O_6 (a) and P_4O_{10} (**b**) cages constituting P_2O_3 (P^{+3}) and P_2O_5 (P^{+5}), respectively[27].

were calibrated to 2152 eV at the white line maximum of the P K-edge XANES spectrum of $NaH_2PO_2 \cdot 2\ H_2O$. The energy step size across the XANES region was 0.2 eV. XANES peaks of our samples show a full width half maximum of ca. 2 eV. P K XANES spectra have been pre- and post-edge background corrected and normalized to the edge jump with the ATHENA program of the IFEFIT package[52].

References

1. Zacharias, M. *et al.* Size-controlled highly luminescent silicon nanocrystals: A SiO/SiO_2 superlattice approach. *Appl. Phys. Lett.* **80,** 661–663 (2002).
2. Böer, K. W. *Survey of Semiconductor Physics, Vol. 2.* (Van Nostrand Reinhold, New York, 1992).
3. Fujii, M., Yamaguchi, Y., Takase, Y., Ninomiya, K. & Hayashi, S. Photoluminescence from impurity codoped and compensated Si nanocrystals. *Appl. Phys. Lett.* **87,** 211919 (2005).
4. Pi, X. D., Gresback, R., Liptak, R. W., Campbell, S. A. & Kortshagen, U. Doping efficiency, dopant location, and oxidation of Si nanocrystals. *Appl. Phys. Lett.* **92,** 123102 (2008).
5. Hao, X. J. *et al.* Effects of phosphorus doping on structural and optical properties of silicon nanocrystals in a SiO_2 matrix. *Thin Sol. Films* **517,** 5646–5652 (2009).
6. Hao, X. J. *et al.* Phosphorus-doped silicon quantum dots for all-silicon quantum dot tandem solar cells. *Solar Energy Mater. & Solar Cells* **93,** 1524–1530 (2009).

7. Perego, M., Bonafos, C. & Fanciulli, M. Phosphorus doping of ultra-small silicon nanocrystals. *Nanotechnology* **21,** 025602 (2010).
8. Khelifi, R. *et al.* Efficient n-type doping of Si nanocrystals embedded in SiO_2 by ion beam synthesis. *Appl. Phys. Lett.* **102,** 013116 (2013).
9. Stegner, A. R. *et al.* Electronic Transport in Phosphorus-Doped Silicon Nanocrystal Networks. *Phys. Rev. Lett.* **100,** 026803 (2008).
10. Stegner, A. R. *et al.* Doping efficiency in freestanding silicon nanocrystals from the gas phase: Phosphorus incorporation and defect-induced compensation. *Phys. Rev. B* **80,** 165326 (2009).
11. Perez-Wurfl, I. *et al.* Si nanocrystal p-i-n diodes fabricated on quartz substrates for third generation solar cell applications. *Appl. Phys. Lett.* **95,** 153506 (2011).
12. Lin, D., Ma, L., Conibeer, G. & Perez-Wurfl, I. Study on electrical properties of Si quantum dots based materials. *Phys. Stat. Sol. B* **248,** 472–476 (2011).
13. Liedke, B., Heinig, K.-H., Mücklich, A. & Schmidt, B. Formation and coarsening of sponge-like Si-SiO_2 nanocomposites. *Appl. Phys. Lett.* **103,** 133106 (2013).
14. Gutsch, S. *et al.* Charge transport in Si nanocrystal/SiO_2 superlattices. *J. Appl. Phys.* **113,** 133703 (2013).
15. Pearson, G. L. & Bardeen, J. Electrical Properties of Pure Silicon and Silicon Alloys Containing Boron and Phosphorus. *Phys. Rev.* **75,** 865–883 (1948).
16. Kambham, A. K., Kumar, A., Florakis, A. & Vandervorst, W. Three-dimensional doping and diffusion in nano scaled devices as studied by atom probe tomography. *Nanotechnology* **24,** 275705 (2013).
17. Koelling, S. *et al.* Direct Imaging of 3D Atomic-Scale Dopant-Defect Clustering Processes in Ion-Implanted Silicon. *Nano Lett.* **13,** 2458–2462 (2013).
18. Norris, D. J., Efros, A. L. & Erwin, S. C. Doped Nanocrystals. *Science* **319,** 1776–1779 (2008).
19. Pereira, R. N., Almeida, A. J., Stegner, A. R., Brandt M. S. & Wiggers, H. Exchange-Coupled Donor Dimers in Nanocrystal Quantum Dots. *Phys. Rev. Lett.* **108,** 126806 (2012).
20. Wagner, C. D., Davis, L. E., Riggs, W. M. The energy dependence of the electron mean free path. *Surf. Interface Anal.* **2,** 53–55 (1980).
21. Brown, G. W. *et al.* Observation of substitutional and interstitial phosphorus on clean Si(100)-(2×1) with scanning tunneling microscopy. *Phys. Rev. B* **72,** 195323 (2005).
22. Ossicini, S. *et al.* Simultaneously B- and P-doped silicon nanoclusters: Formation energies and electronic properties. *Appl. Phys. Lett.* **87** 173120 (2005).
23. Dalpian, G. M. & Chelikowsky, J. R. Self-Purification in Semiconductor Nanocrystals. *Phys. Rev. Lett.* **96,** 226802 (2006).
24. Dalpian, G. M. & Chelikowsky, J. R. Dalpian and Chelikowsky Reply: *Phys. Rev. Lett.* **100,** 179703 (2008).
25. Chan, T.-L., Tiago, M. L., Kaxiras, E. & Chelikowsky, J. R. Size Limits on Doping Phosphorus into Silicon Nanocrystals. *Nano Lett.* **8,** 596–600 (2008).
26. Nicollian, E. H. & Brews, J. R. MOS (*Metal Oxide Semiconductor) Physics and Technology*. (Wiley-Interscience, New York, 1982).
27. Holleman, A. F., Wiberg, E. & Wiberg, N. Lehrbuch der Anorganischen Chemie. [101st Ed] (Walter deGruyter, Berlin, 1995). in German.
28. Zimina, A., Eisebitt, S., Eberhardt, W., Heitmann, J. & Zacharias, M. Electronic structure and chemical environment of silicon nanoclusters embedded in a silicon dioxide matrix. *Appl. Phys. Lett.* **88,** 163103 (2006).
29. Gutsch, S. *et al.* Doping efficiency of phosphorus doped silicon nanocrystals embedded in a SiO_2 matrix. *Appl. Phys. Lett.* **100,** 233115 (2012)
30. Singh, A. & Davis, E. A. THE SiO_x:H_y THIN FILM SYSTEM II. Optical bandgap behavior. *J. of Non-Cryst. Sol.* **122,** 233–240 (1990).
31. König, D., Rudd, J., Green, M. A. & Conibeer, G. Role of the Interface for the Electronic Structure of Silicon Quantum Dots. *Phys. Rev. B* **78,** 035339 (2008).
32. Gnaser, H. *et al.* Phosphorus doping of Si nanocrystals embedded in silicon oxynitride determined by atom probe tomography. *J. Appl. Phys.* **115,** 034304 (2014).
33. Lannoo, M., Delerue, C. & Allan, G. Theory of radiative and nonradiative transitions for semiconductor nanocrystals. *J. Luminescence* **70,** 170–184 (1996).
34. Sze, S. M. & Ng, K. K. *Physics of Semiconductor Devices*, 3rd Ed. (Wiley, 2007).
35. Trupke, T. *et al.* Temperature dependence of the radiative recombination coefficient of intrinsic crystalline silicon. *J. Appl. Phys.* **94,** 4930–4937 (2003).
36. Richter, A., Glunz, S. W., Werner, F., Schmidt, J. & Cuevas, A. Improved quantitative description of Auger recombination in crystalline silicon. *Phys. Rev. B* **86,** 165202 (2012).
37. Fujii, M., Yamaguchi, Y., Takase, Y., Ninomiya, K. & Hayashi, S. Control of photoluminescence properties of Si nanocrystals by simultaneously doping n- and p-type impurities. *Appl. Phys. Lett.* **85,** 1158–1160 (2004).
38. Faulkner, R .A. Higher donor excited states for prolate-spheroid conduction bands: A re-evaluation of silicon and germanium. *Phys. Rev.* **184,** 713–721 (1969).
39. König, D., Hiller, D., Gutsch, S. & Zacharias, M. Energy Offset Between Silicon Quantum Structures: Interface Impact of Embedding Dielectrics as Doping Alternative. *Adv. Mater. Interfaces* **1,** 1400359 (2014).
40. Becke, D. Density-functional exchange-energy approximation with correct asymptotic behaviour. *Phys. Rev. A* **38,** 3098–3100 (1988).
41. Lee, C., Yang, W. & Parr, R. G. Density-functional exchange-energy approximation with correct asymptotic behaviour. *Phys. Rev. B* **37,** 785–789 (1988).
42. Hehre, W. J., Ditchfield, R. & Pople, J. A. Self-Consistent Molecular Orbital Methods. 12. Further extensions of Gaussian-type basis sets for use in molecular-orbital studies of organic-molecules. *J. Chem. Phys.* **56,** 2257–2261 (1972).
43. Francl, M. M. *et al.* Self-Consistent Molecular Orbital Methods. 23. A polarization-type basis set for 2nd-row elements. *J. Chem. Phys.* **77,** 3654–3666 (1982).
44. Rassolov, V. A., Ratner, M. A., Pople, J. A., Redfern, P. C. & Curtiss, L. A. 6-31G* Basis Set for Third-Row Atoms. *J. Comp. Chem.* **22,** 976–984 (2001).
45. Frisch, M.J. *et al. Gaussian03, Revision D.02*, (Gaussian Inc., Wallingford, CT, (2004), Date of access: 28/11/2014; http://www.gaussian.com/g_misc/g03/citation_g03.htm.
46. Frisch, M.J. *et al. Gaussian09, Revision A.02*, (Gaussian Inc., Wallingford, CT, (2010), Date of access: 28/11/2014; http://www.gaussian.com/g_tech/g_ur/m_citation.htm
47. König, D., Rudd, J., Green, M. A. & Conibeer, G. Critical Discussion of Computation Accuracy. supplemental material to *Phys. Rev. B* **78,** 035339 (2008), Date of access: 28/11/2014; http://journals.aps.org/prb/abstract/10.1103/PhysRevB.78.035339.
48. Krukau, A. V., Vydrov, O. A., Izmaylov, A. F. & Scuseria, G. E. Influence of the exchange screening parameter on the performance of screened hybrid functionals. *J. Chem. Phys.* **125,** 224106 (2006).
49. Becke, A. D. & Johnson, E. R. A simple effective potential for exchange. *J. Chem. Phys.* **124,** 221101 (2006).

50. Koller, D., Tran, F. & Blaha, P. Improving the modified Becke-Johnson exchange potential. *Phys. Rev. B* **85,** 155109 (2012).
51. Perdew, J. P., Burke, K. & Ernzerhof, M. Generalized gradient approximation made simple, *Phys. Rev. Lett.* **77,** 3865–3868 (1996).
52. Ravel, B. & Neville, M. ATHENA, ARTEMIS, HEPHAESTUS: data analysis for X-ray absorption Spectroscopy using IFEFFIT. *J. Synchrotron Radiation* **12,** 537–541 (2005).
53. Franke, R. & Hormes, J. The P K-near edge absorption spectra of phosphates. *Physica B* **216,** 85–95 (1995).

Acknowledgments

D.K. acknowledges use of compute cluster Leonardi, engineering faculty, UNSW, and financial support by Australian Government via Australian Renewable Energy Agency (ARENA). Australian government does not accept responsibility for any information expressed herein. D.H. acknowledges funding by the German Research Foundation (DFG) under grant number HI 1779/3-1. D.K., S.G. and D.H. acknowledge DAAD-Go8 joint research cooperation schemes (54385434 and 57060437). The ANKA Synchrotron Radiation Facility is acknowledged for providing beamtime.

Author Contributions

D.K. developed concepts, carried out h-DFT calculations, participated in characterisation data post processing and drafted manuscript. S.G. and D.H. processed samples and participated in sample characterisation and data post processing. H.G., M.K., M.W., J.G. and R.S. characterized samples and processed associated data. D.H., D.K. and M.Z. guided the project. All authors discussed and revised the manuscript.

Additional Information

Competing financial interests: The authors declare no competing financial interests.

How to cite this article: König, D. *et al.* Location and Electronic Nature of Phosphorus in the Si Nanocrystal – SiO_2 System. *Sci. Rep.* **5,** 9702; doi: 10.1038/srep09702 (2015).